Turbomachinery Rotor Forces

Final Report

Contract NAS8-33108 (October 30, 1978 - August 30, 1988)

prepared by

Norbert Arndt

Approved by

Allan J. Acosta
Christopher E. Brennen
Thomas K. Caughey

August 30, 1988

1. INTRODUCTION

The overall objective of this contract was to experimentally and theoretically evaluate the fluid–induced forces, both steady and unsteady, acting upon an impeller of a centrifugal pump, and to investigate impeller blade–diffuser vane interaction in centrifugal pumps with vaned radial diffusers. Knowledge of the steady and unsteady forces, and the associated rotordynamic coefficients, is required to effectively model the rotordynamics of high speed turbopumps such as the High Pressure Oxygen Turbopump (HPOTP) and the High Pressure Fuel Turbopump (HPFTP) of the Space Shuttle Main Engine (SSME). Under the sponsorship of this contract, an extensive investigation of these forces and rotordynamic coefficients using different impellers in combination with volutes and vaned diffusers, and axial inducers has been conducted. These rotor forces are global, i.e., they result from the pressure distribution acting upon the complete impeller. Local forces and pressures are also important in impeller–diffuser interaction, for they may cause cavitation damage and even vane failure. Thus, in a separate investigation, impeller wake, and impeller blade and diffuser vane pressure measurements were made.

This research program was begun on October 30, 1978, and completed August 30, 1988. A special test facility was designed and constructed for this work. In what follows the nature of the rotordynamic forces is discussed, the experimental facility is described, and measurements of unsteady forces and pressures are reported together with a brief and incomplete attempt to calculate these flows. A summary of all publications and reports issued under this contract is included.

2. IMPELLER FLUID FORCES

2.1. Notation

First, a few notes on notation will be presented. The ensemble averaged forces in the laboratory frame are decomposed into forces F_x and F_y in the x and y directions shown in figure 1. Like all other forces these are nondimensionalized with the term $\rho \pi \omega^2 r_2^3 b_2$, where ρ is the fluid density, ω the rotational frequency (radian frequency), and r_2 and b_2 are the discharge radius and the discharge width of the impeller. The x and y coordinates are nondimensionalized using the impeller discharge radius, r_2. In the experiments, a circular whirl motion, with a radius ϵ and at a whirl frequency Ω, is superimposed on the impeller. The nondimensionalized ensemble averaged forces F_x and F_y are decomposed into their steady and ensemble averaged unsteady parts as follows:

$$\begin{pmatrix} F_x \\ F_y \end{pmatrix} = \begin{pmatrix} F_{0x} \\ F_{0y} \end{pmatrix} + [A] \begin{pmatrix} x/r_2 \\ y/r_2 \end{pmatrix} = \begin{pmatrix} F_{0x} \\ F_{0y} \end{pmatrix} + [A(\Omega/\omega)] \begin{pmatrix} (\epsilon/r_2)\cos\Omega t \\ (\epsilon/r_2)\sin\Omega t \end{pmatrix}, \qquad (1)$$

where F_{0x} and F_{0y} are the time–averaged mean of F_x and F_y, and therefore represent the steady component of the radial forces. $[A]$ is the hydrodynamically–induced force matrix which depends upon the frequency ratio, (Ω/ω). Note that the second form of equation (1) is specific to the circular whirl orbits used in the present experiments. The conventional approach of the rotordynamicists is to represent this dependence on the frequency ratio (Ω/ω) by subdividing the matrix into components which depend upon the orbit position (x, y), the orbit velocity $(\dot{x}, \dot{y})$, and the orbit acceleration $(\ddot{x}, \ddot{y})$. Thus, the common

1

notation is

$$\begin{pmatrix} F_x \\ F_y \end{pmatrix} = \begin{pmatrix} F_{0x} \\ F_{0y} \end{pmatrix} - [M] \begin{pmatrix} \ddot{x} \\ \ddot{y} \end{pmatrix} - [C] \begin{pmatrix} \dot{x} \\ \dot{y} \end{pmatrix} - [K] \begin{pmatrix} x \\ y \end{pmatrix}, \tag{2}$$

where the matrices $[M]$, $[C]$, and $[K]$ are the hydrodynamically–induced mass, damping, and stiffness matrices. It then follows that

$$A_{xx} = -K_{xx} - (\Omega/\omega)C_{xy} + (\Omega^2/\omega^2)M_{xx}, \tag{3.1}$$

$$A_{xy} = -K_{xy} + (\Omega/\omega)C_{xx} + (\Omega^2/\omega^2)M_{xy}, \tag{3.2}$$

$$A_{yx} = -K_{yx} - (\Omega/\omega)C_{yy} + (\Omega^2/\omega^2)M_{yx}, \tag{3.3}$$

$$A_{xx} = -K_{yy} + (\Omega/\omega)C_{yx} + (\Omega^2/\omega^2)M_{yy}. \tag{3.4}$$

It should however be noted that our measurements indicate that the matrix elements of the force matrix $[A]$ often depart substantially from the quadratic form implied by the above definitions (2.3). Finally, it should be noted that the definition of the force matrix (see equation (1)) implies

$$F_N = (1/2)(A_{xx} + A_{yy}) \quad \text{and} \quad F_T = (1/2)(-A_{xy} + A_{yx}), \tag{4}$$

where F_N and F_T are the mean, i.e., averaged over the whirl orbit, forces normal and tangential to the whirl orbit (figure 1). Since virtually all experimentally measured force matrices $[A]$ were skew–symmetric with $F_N = A_{xx} = A_{yy}$ and $F_T = -A_{xy} = A_{yx}$, the discussion of the hydrodynamically–induced force matrix $[A]$ will be confined to the physically interpretable unsteady force components F_N and F_T.

2.2. Experimental Facility

A detailed description of the test facility, a recirculating water pump loop, closed to atmosphere, can be found in many of the references (2.2, 2.3, 2.7, 2.10 and 2.11). The experiments were conducted in the test section of this facility, the Rotor Force Test Facility (RFTF), shown in figure 2. Briefly, the RFTF consists of a housing which can accommodate different impeller/volute (diffuser) configurations. The experimental objective of the rotordynamic experiments was to impose well controlled rotations and whirl motions on a very stiff impeller/shaft system and to measure directly the resulting force on the impeller. The prescribed motions were produced as follows. The normal rotational motion is driven by a 20 horse power DC motor through the main pump shaft. This rotates in a double bearing cartridge in which the outer bearings are set eccentrically to the inner bearings. Hence, rotation of the intermediate cartridge by means of a 2 horse power DC "whirl" motor rotating a drive sprocket by means of a toggled belt produces the superimposed whirl motion. All of the experiments described herein were conducted with a radius of 0.0495 in. for the whirl motion. During the last stage of the contract work, however, the the eccentric drive mechanism has been rebuilt to permit testing with the radius of the whirl orbit adjustable from 0.000 in. to 0.060 in. The maximum main shaft speed is about 3600 rpm, the maximum whirl speed about 1800 rpm.

Both the main motor and the whirl motor are position and velocity controlled using optical encoders mounted on each shaft. The entire control system is also integrated into the data acquisition system. Both the motor control system and the data taking system are in detail described in references 2.7 and 2.11.

The forces on an impeller mounted on a rotor may be measured in two ways:
- (a) in a frame rotating with the rotor,
- (b) in a stationary frame.

The experimental research program began with force measurements using an externally mounted stationary force balance (1.3, 1.5 and 2.2). The results were obtained by slowly moving the impeller center around the circular orbit, that is to say quasi–statically. Hence, only the steady force components, F_{0x} and F_{0y}, and the hydrodynamically–induced stiffness matrix, $[K]$, could be measured. The force balance, consisting of three strain-gaged aluminum load cells, was used with the entire impeller–eccentric drive system floating on soft spring supports attached to the ceiling. Two of the strain–gaged load cells were mounted horizontally for measurements of the horizontal force and the torque, the third load cell measured the vertical force. The findings those measurements permitted an "educated" design of a rotating dynamometer, mounted on the main shaft directly behind the impeller. Therefore, it measures directly the forces on the impeller. The four–post design of this rotating dynamometer involved 9 strain–gage bridges which measure all six force components on the impeller. A detailed description is given in reference 2.7. The signals are lead through a slip–ring assembly to the data acquisition system. This rotating dynamometer permitted measurements of the rotordynamic force matrix $[A]$ due to the impeller fluid forces.

Furthermore, measurements were made of the circumferential pressure distribution in the flow leaving the impeller and in the leakage passage between the impeller shroud and the casing (2.3). Integration of those pressure distributions yielded radial forces acting on the impeller discharge and on the shroud. Due to the limited frequency response of the water manometers used for these pressure measurements, only steady radial forces and stiffness matrices $[K]$ could be obtained from these experiments.

The impeller discharge was sealed from the impeller intake by means of an adjustable face seal. During all measurements, this seal was backed off to some desirable clearance, usually 0.005 in., to avoid interference with the force measurements. Hence, all tests involved a small leakage flow back from the impeller discharge to the impeller inlet between the impeller shroud and the casing (for a seal clearance of 0.005 in., the leakage flow rate at design flow was estimated to be about 2% of the design flow rate (2.2)). The results indicate that both the leakage flow and the main impeller through–flow contribute to the steady force and the rotordynamic force matrix.

During the experimental investigation, several impeller/volute(diffuser) configurations were tested. A complete description of those impellers and volutes can be found in references 2.3, 2.7 and 2.10. The impellers most important for the discussion of the results are a five–bladed centrifugal impeller, referred to as Impeller X, a two–dimensional model of that impeller, referred to as Impeller Z, and one half of the double–suction impeller of the High Pressure Oxygen Turbopump (HPOTP) of the Space Shuttle Main Engine (SSME),

3

referred to as Impeller R. The centrifugal impellers were tested most thoroughly with a spiral volute, Volute A, designed to be well matched with Impeller X at a flow coefficient, $\phi = 0.092$ (the flow coefficient, ϕ, is defined as the flow rate, Q, nondimensionalized by the impeller discharge area, A_2, and the impeller tip speed, u_2, i.e. $\phi = Q/(A_2 u_2)$). The SSME impeller was tested most thoroughly with Volute E, a volute with seventeen circular arc vanes and an elliptical cross section. This volute was provided by the Rocketdyne Division of Rockwell International, and is similar to the volute used in the Space Shuttle Main Engine. Since the behavior of the unsteady forces F_N and F_T with whirl ratio was different for the SSME impeller and the centrifugal impellers several existing axial inducers were tested as well (note that the SSME impeller has an inducer).

Detailed descriptions of the experimental facility can be found in references 2.2, 2.3, 2.5, 2.6, 2.7, 2.10 and 2.11.

2.3. Force Measurements in the Stationary Frame

The experimental research program began with force measurements using an externally mounted stationary force balance. The results were obtained by slowly moving the impeller center around a circular orbit ($(\omega/\Omega) \ll 1$), that is to say quasi–statically. Hence, only the steady force components, F_{0x} and F_{0y}, and the hydrodynamically–induced stiffness matrix, $[K]$, could be measured (1.3, 1.5 and 2.2).

The main finding of this first stage of the experimental investigation, using Impeller X and Volute A, was that the hydrodynamically–induced stiffness matrix $[K]$ is statically unstable. The direct stiffness terms (K_{xx} and K_{yy}) were found to be equal in magnitude and to have the same negative sign, resulting in a fluid force radially outward. The cross–coupled stiffness terms (K_{xy} and K_{yx}) were found to be equal in magnitude, and their opposite signs were such to produce a tangential fluid force capable of driving forward whirl motion of the impeller, should the system lack adequate damping. This work was reported in references 1.3, 1.5, 2.1 and 2.2.

2.4. Force Measurements using a Rotating Dynamometer

In the second stage of the experimental investigation, measurements of the steady and unsteady fluid forces on pump impellers were made using a rotating dynamometer mounted directly behind the impeller (2.7 and 2.11). The objective was to study the behavior of the hydrodynamically–induced force matrix $[A]$ for different impeller/volute (diffuser) configurations, and under different operating conditions, i.e., different whirl ratios, flow coefficients, and cavitation numbers. To discuss all the data obtained would by far exceed the scope of this final report. Instead, a cross section of the experimental results will be presented highlighting the most important phenomena. A complete discussion of all the results obtained in the course of this research can be found in the publications, theses and contract reports that originated from this work (see the enclosed list of publications and contract reports).

The most important results of this research are:

For Impeller X and Volute A, the steady force had a minimum at the design flow coefficient, i.e., the impeller and the volute were well matched. That was not so for the impeller of the High Pressure Oxygen Turbopump (HPOTP) of the Space Shuttle Main

4

Engine (SSME), Impeller R, and a volute closely resembling the volute used in the HPOTP of the SSME. The steady radial force was found to be nearly independent of flow coefficient. Thus, Impeller R and Volute E are not well matched from the viewpoint of minimizing the steady radial force for the design or the best efficiency flow coefficient (1.11 and 2.4).

Turning to the unsteady forces, F_N and F_T, a region of forward whirl for which the average tangential force is destabilizing, i.e., in the same direction as the whirl motion, was found for all impeller/volute (diffuser) combinations tested. In general the region of forward whirl for which the tangential force was destabilizing increased with the flow coefficient decreasing from maximum flow. For low flow coefficients, the tangential force, depending on the volute (diffuser) used, may become a strong function of whirl ratio, to the extent that F_T has several zero crossings; e.g., the curve F_T versus (Ω/ω) resembles a cubic. For Impeller X and Volute E (i.e., a centrifugal impeller and a volute with a vaned diffuser), it has even been observed that for a very low flow coefficient a region of reverse whirl became destabilizing (1.11, 1.15, 2.4 and 2.7), whereas normally reverse whirl is stable.

For the impeller of the HPOTP (Impeller R), an impeller with an axial inducer, the appearance of the cubic for the tangential force, F_T, at low flow coefficients was independent of the volute used for testing. The occurrence of flow reversal in the intake upstream of the inducer seems to coincide with the transition of F_T (1.15 and 2.4).

To investigate the influence the axial inducer may have on this peculiar behavior, several axial inducers were tested. For low flow coefficients, the curve F_T versus (Ω/ω) had multiple zero crossings for forward whirl. Hence, the axial inducer may have significant influence on the behavior of the tangential force for low flow coefficients (2.5).

Exposing the annular region surrounding the impeller shroud to the housing reservoir (i.e., shortening the front shroud of the casing) reduced the forces, both the steady and the unsteady, on the impeller (these test were done for Impeller X and Volute A). Also, the region of destabilizing forward whirl was reduced. This clearly indicates the importance of the flow in the rotating impeller shroud/stationary casing region for the steady and unsteady forces on the impeller (1.12 and 2.6).

In a subsequent experiment, force measurements were made for a two–dimensional model of Impeller X, Impeller Z, and Volute A (since the impeller is truly two–dimensional, no part of the external front shroud could contribute to the steady radial forces or to the force matrix [A]). The steady radial force and elements of the hydrodynamically–induced force matrix were much smaller than for Impeller X and agreed well with the theory of references 1.12 and 1.13. These results again clearly indicate the importance of the flow in the impeller shroud/casing region for the steady and unsteady forces on the impeller (1.12 and 2.6).

The effect of cavitation upon the forces experienced by a whirling centrifugal impeller were examined using Impeller X and Volute A. Some preliminary results have been published in reference 1.15. The measurements showed that for the design flow coefficient the magnitude of the steady radial force varied less that 10% from flow without cavitation to flow with a significant head loss of 19% due to cavitation. Data for the unsteady forces F_N and F_T taken at the design flow coefficient were presented for noncavitating flow and flow with 3% head loss due to cavitation. The magnitudes of both F_N and F_T changed

5

only slightly with cavitation, and the region of destabilizing whirl was not altered by the 3% head loss. More data on the effect of cavitation on a whirling centrifugal impeller will be presented in reference 2.11.

The force measurements using the rotating dynamometer were published in references 1.4, 1.7, 1.9, 1.11, 1.15, 1.18, 2.4, 2.5, 2.6, 2.7, 2.9 and 2.11.

2.5. Pressure Measurements of the Flow Leaving the Impeller

Steady pressure measurements were made at two axial locations on the stationary casing facing the rotating impeller shroud. The hydrodynamic stiffness matrices obtained from those measurements showed clearly, that the flow in the annular region between the impeller shroud and the casing does significantly contribute to the stiffness matrices measured with the rotating dynamometer for the entire impeller (2.3). Results of the steady pressure measurements are in addition to reference 2.3 also published in references 1.8, 1.12, and 2.7.

2.6. Moment Measurements using a Rotating Dynamometer

As yet, only force measurements in a direction perpendicular to the axis of rotation (the so called radial forces) have been discussed. However, the rotating dynamometer measures all six components of the dynamic or unsteady forces in the rotating frame, and inspection of those leads to some further insights into the hydrodynamically–induced forces occurring in a pump. Analogous to the forces, the ensemble averaged moments, M_x and M_y, are decomposed into their steady and their unsteady part as follows:

$$\begin{pmatrix} M_x \\ M_y \end{pmatrix} = \begin{pmatrix} M_{0x} \\ M_{0y} \end{pmatrix} + [B] \begin{pmatrix} x/r_2 \\ y/r_2 \end{pmatrix} = \begin{pmatrix} M_{0x} \\ M_{0y} \end{pmatrix} + [B(\Omega/\omega)] \begin{pmatrix} (\epsilon/r_2)\cos\Omega t \\ (\epsilon/r_2)\sin\Omega t \end{pmatrix}, \quad (5)$$

where M_{0x} and M_{0y} are the time–averaged mean of M_x and M_y, and therefore represent the steady component of the bending moments. $[B]$ is the hydrodynamically–induced moment matrix, depending upon the frequency ratio, (Ω/ω). Note that the second form of equation (5) is specific to the circular whirl orbits used in the present experiments. The mean moments normal and tangential to the whirl orbit, M_N and M_T are given by:

$$M_N = (B_{xx} + B_{yy})/2 \quad \text{and} \quad M_T = (B_{yx} - B_{xy})/2 \quad (6)$$

The data discussed were taken for the Impeller X/Volute A combination. The steady moments indicated that the lines of action of the steady radial forces are forward of the impeller discharge (2.9). The reason the lines of action are forward of the impeller discharge is the contribution to the steady force from the pressure distribution on the exterior of the shroud which combines with the force on the discharge to yield the steady radial force. These components were measured and compared in references 1.12 and 2.3. Since the force on the exterior of the shroud is comparable to the force on the discharge the line of action of the combination will be forward of the center of the discharge. Similar to the force matrix, the moment matrix $[B]$ was found to be "skew–symmetric", i.e., $B_{xx} = B_{yy}$ and $B_{xy} = -B_{yx}$. Thus, it suffices to discuss M_N and M_T (2.9). Analyzing the unsteady moments, it was found that the lines of action of the unsteady forces F_N and F_T are

significantly closer to the impeller discharge than the lines of action of the steady forces. Hence, the contribution of the flow in the annular region between the rotating impeller shroud and the casing to the force matrices is not as strong as to the steady force. The moment measurements using the rotating dynamometer were published in reference 2.9.

2.7. Theoretical Work on the Whirling Impeller Flow

Parallel to the experimental investigations, theoretical work on whirling impeller flow was carried out. Two different approaches were taken. The model used by Adkins (1.12 and 2.3) is a quasi–one–dimensional one, requiring as input data only the geometry of the impeller and the volute and the impeller/volute performance curve. Qualitatively good predictions of both the steady radial force and the rotordynamic force matrices was achieved. The theory furthermore permitted one to investigate the various sources of contribution to the rotor forces. It was found that the radial forces on the impeller are primarily due to the asymmetric pressure distribution at the impeller discharge and not to the asymmetric momentum distribution at the impeller discharge.

The model used by Tsujimoto et al. (1.6 and 1.13) is a two–dimensional, linearized vorticity flow. Again, good qualitative agreement of both the steady and the unsteady forces was achieved. From a quantitative standpoint, Tsujimoto's model was slightly better. It also does not impose any restriction on the range of frequency ratios (as Adkins model does). The same theory also can be used to account for rotating stall and for a diffuser pump configuration (1.6).

The theoretical work on impeller fluid forces was published in references 1.6, 1.8, 1.13 and 2.3.

3. WAKE MEASUREMENTS AND IMPELLER BLADE–DIFFUSER VANE PRESSURE MEASUREMENTS

The impeller blade–diffuser vane interaction in centrifugal pumps with vaned diffusers may be divided into two different mechanisms; potential flow interaction and wake interaction. The potential flow interaction between two blade rows moving relative to each other arises because of the circulation about the blades and because of potential fields, other than circulation, about the blades that are due to the finite thickness of the blades. The potential fields about a blade extend both upstream and downstream of the blade. The wake interaction refers to the unsteadiness induced at a blade of a blade row by wakes shed by the blades of an upstream blade row and convected downstream. If the radial gap between the impeller blades and the diffuser vanes is small, i.e., a small percentage of the impeller discharge radius, both interaction mechanisms will occur simultaneously, and may influence each other.

3.1. Test Facility and Instrumentation

The experiments were conducted in the same test facility as the impeller force measurements. The impellers and diffusers used for the steady and unsteady measurements are described in detail in reference 2.10. For the unsteady pressure measurements, piezo-electric pressure transducers from PCB Inc. were used. For the flow angle measurements, a three–hole tube was designed, built and calibrated (2.10).

7

3.2. Discussion of Results

Steady and unsteady measurements of the flow discharged from an impeller into a vaneless diffuser were made for two different impellers, one half of the double suction impeller of the High Pressure Oxygen Turbopump (HPOTP) of the Space Shuttle Main Engine (SSME) and a two-dimensional test impeller. The objective of those measurements was to quantify the magnitude of the flow nonuniformities at the impeller discharge due to the wakes shed by the impeller blades, and to quantify how rapidly these nonuniformities decay with increasing radial distance from the impeller discharge. In particular, the measurements were aimed at investigating the nonuniformities of the flow in vaneless diffusers at radial distances to the impeller discharge comparable to the radial gaps commonly found in diffuser pumps. These measurements were made using a total pressure probe and a three-hole tube. The total pressure measurements showed that the total pressure fluctuations very close to the impeller discharge can be as large as the total pressure rise across the pump. Furthermore, the three-hole tube measurements showed significant total pressure, pressure and flow angle fluctuations occurring at radial distances downstream of the impeller discharge corresponding to locations where the diffuser inlet is located in vaned diffusers. Hence, the diffuser vanes have to be expected to experience pressure fluctuations due to the impinging wakes shed by the impeller blades (2.10).

Next, the interaction between impeller blades and diffuser vanes in diffuser pumps was investigated. Steady and unsteady pressure measurements were made on the diffuser vanes and on the front shroud wall of a vaned and a vaneless diffuser. Two different impellers were used, one half of the impeller of the double suction pump of the HPOTP of the SSME, and a two-dimensional impeller. The measurements were made for different flow coefficients, shaft speeds, and radial gaps between the impeller blades and the diffuser vanes (1.5% and 4.5% of the impeller discharge radius for the impeller of the HPOTP, and 5% and 8% for the two-dimensional impeller). The vane pressure fluctuations were larger on the vane suction side than on the vane pressure side attaining their maximum value, of the same order of magnitude as the total pressure rise across the pump, near the leading edge. The resulting lift on the vane, both steady and unsteady was computed from the pressure measurements at mid vane height. The magnitude of the fluctuating lift was found to be larger than the steady lift. For the impeller of the HPOTP, pressure measurements on the front shroud of a vaned and a vaneless diffuser showed that the front shroud pressure fluctuations increased with the presence of the diffuser vanes. Lift, vane and front shroud pressure fluctuations decreased strongly with increasing radial gap (1.10,1.16 and 2.10).

Unsteady impeller blade pressure measurements were made for a second two-dimensional impeller with blade number and blade geometry identical to the two-dimensional impeller for the wake and the diffuser vane pressure measurements. The largest blade pressure fluctuations, of the same magnitude as the large pressure fluctuations on the vane suction side, occurred at the blade trailing edge. However, the dependence of the fluctuations on the flow coefficient was found to be different for the impeller blades and the diffuser vanes; on the vane suction side, the fluctuations were largest for maximum flow and decreased with decreasing flow coefficient, whereas at the blade trailing edge, the fluctuations were smallest for maximum flow and increased with decreasing flow coefficient. Increasing the number of the diffuser vanes resulted in a significant decrease of the impeller

8

blade pressure fluctuations (1.14 and 2.10).

Results of the wake measurements and the impeller–diffuser vane pressure measurements were published in references 1.10, 1.14, 1.16, 1.17, 1.19 and 2.10.

3.3. Numerical Simulation of Impeller Blade–Diffuser Vane Interaction

In collaboration with the NASA Ames Research Center, a numerical simulation of the impeller–diffuser interaction for the two–dimensional impeller was attempted. A computer code written by M.M. Rai for axial turbine rotor–stator interaction solving the unsteady, two–dimensional, turbulent, thin–layer Navier–Stokes equations was used. Due to the different geometry, radial flow versus axial flow, several modifications had to be made to the program. Although the program has advanced to a stage where the code executes, numerically convergent results have as yet not been obtained. At this point, the following items seem to need improvement for the program to give numerically convergent results: finding the proper set of boundary conditions, i.e., the proper mix of reflective and non-reflective boundary conditions such that pressure waves as they occur during the start of the computation can "leave" the computational domain, and moving the numerical inlet and outlet boundaries significantly further away from the impeller inlet and the diffuser outlet such that the flow fluctuations due to the rotor–stator interaction have decayed at the numerical boundaries. The latter modification may make it necessary to either use the three–dimensional version of the code or to add some subroutines to the code that permit a stream surface approach for the inlet and the outlet sections (no publications or reports are available on that work as yet).

APPENDIX A (LIST OF PUBLICATION AND REPORTS)

The following publications and reports were all generated with the full or partial support of the present contract.

Publications

1.1 Brennen, C.E., Acosta, A.J., and Caughey, T.K., "A Test Program to Measure Fluid Mechanical Whirl-Excitation Forces in Centrifugal Pumps," Proc. First Workshop on Rotordynamic Instability Problems in High-Performance Turbomachinery, Texas A&M University, May 12-14, 1980, pp. 229-236.

1.2 Chamieh, D., Acosta, A.J., Brennen, C.E., and Caughey, T.K., "A Brief Note on the Interaction of an Actuator Cascade with a Singularity," Proc. First Workshop on Rotordynamic Instability Problems in High-Performance Turbomachinery, Texas A&M University, May 12-14, 1980, pp. 237-248.

1.3 Chamieh, D., Acosta, A.J., Brennen, C.E., and Caughey, T.K., and Franz, R., "Experimental Measurements of Hydrodynamic Stiffness Matrices for a Centrifugal Pump Impeller," Proc. Second Workshop on Rotordynamic Instability Problems in High-Performance Turbomachinery, Texas A&M University, May 10-12, 1982, NASA Conf. Publ. 2250, pp. 382-398.

1.4 Jery, B., Acosta, A.J., Brennen, C.E., and Caughey, T.K., "Hydrodynamic Impeller Stiffness, Damping and Inertia in the Rotordynamics of Centrifugal Pumps," Third Workshop on Rotordynamic Instability Problems in High-Performance Turbomachinery, Texas A & M University, 1984, NASA Conf. Publ. 2338, pp. 137-160.

1.5 Chamieh, D.S., Acosta, A.J., Brennen, C.E., and Caughey, T.K., "Experimental Measurements of Hydrodynamic Radial Forces and Stiffness Matrices for a Centrifugal Pump-Impeller," ASME Journal of Fluids Engineering, Vol. 107, Sept. 1985, pp. 307-315.

1.6 Tsujimoto, Y., Acosta, A.J., and Brennen, C.E., "A Theoretical Study of Impeller and/or Vaneless Diffuser Attributed Rotating Stalls and Their Effects on the Whirling Instability of a Centrifugal Impeller," Journal Japanese Mech. Eng. Soc., 1986, Vol. 52, No. 483, pp. 3747-3754 (in Japanese).

1.7 Brennen, C.E., Acosta, A.J., and Caughey, T.K., "Impeller Fluid Forces," NASA Proc. Advanced Earth-to-Orbit Propulsion Technology Conference, Huntsville, Al., May 1986, pp. 270-295.

1.8 Adkins, D.R., and Brennen, C.E., "Origins of Hydrodynamic Forces on Centrifugal Pump Impellers," Proc. of Fourth Workshop on Rotordynamic Instability Problems in High–Performance Turbomachinery, June 2–4, 1986, NASA Conf. Publ. 2443, pp. 467–491.

1.9 Franz, R.J., Brennen, C.E., Acosta, A.J., and Caughey, T.K., "On the Effects of Cavitation on the Radial Forces and Hydrodynamic Stiffness of a Centrifugal Pump," Proc. of Fourth Workshop on Rotordynamic Instability Problems in High–Performance Turbomachinery, June 2–4, 1986, NASA Conf. Publ. 2443, pp. 493–501.

1.10 Arndt, N., Acosta, A.J., Brennen, C.E., and Caughey, T.K., "Unsteady Diffuser Vane and Impeller Wake Pressure Measurements in a Centrifugal Pump," Proc. of the Eighth Conference on Fluid Machinery, Akademiai Kiado, 1987, Budapest, Vol. 1, pp. 49–56.

1.11 Franz, R., Arndt, N., Acosta, A.J., Brennen, C.E., and Caughey, T.K., "Rotordynamic Forces on Centrifugal Impellers," Proc. of the Eighth Conference on Fluid Machinery, Akademiai Kiado, 1987, Budapest, Vol. 1, pp. 252–258.

1.12 Adkins, D.R., and Brennen, C.E., "Analyses of Hydrodynamic Radial Forces on Centrifugal Pump Impellers," ASME Journal Fluids Engineering, 1988, Vol. 110, No. 1, pp. 20–28.

1.13 Tsujimoto, Y., Acosta, A.J., and Brennen, C.E., "Theoretical Study of Fluid Forces on a Centrifugal Impeller Rotating and Whirling in a Volute," ASME Journal of Vibration, Acoustics, Stress and Reliability in Design, July 1988, Vol. 110, No. 3, pp. 263–269.

1.14 Brennen, C.E., Franz, R., and Arndt, N., "Rotor/Stator Unsteady Pressure Interaction," Proc. Third Earth–to–Orbit Conference, Huntsville, Al., May 1988.

1.15 Brennen, C.E., Franz, R., and Arndt, N., "Effects on Cavitation on Rotordynamic Force Matrices," Proc. Third Earth–to–Orbit Conference, Huntsville, Al., May 1988.

1.16 Arndt, N., Acosta, A.J., Brennen, C.E., and Caughey, T.K., "Rotor-Stator Interaction in a Diffuser Pump," 33rd ASME International Gas Turbine and Aeroengine Congress (88-GT-55 paper), Amsterdam, June 1988, and to appear in the ASME Journal of Turbomachinery.

1.17 Arndt, N., Acosta, A.J., Brennen, C.E., and Caughey, T.K., "Experimental Investigation of Rotor-Stator Interaction in a Centrifugal Pump with Different Vaned Diffusers," in preparation to be submitted for presentation at the 34th ASME International Gas Turbine and Aeroengine Congress, Toronto, June 1989.

1.18 Franz, R., Acosta, A.J., Brennen, C.E., and Caughey, T.K., "The Effects of Cavitation on the Rotordynamic Forces on a Centrifugal Impeller," in preparation to be submitted for presentation at the Pumping Machinery Symposium at the Third Joint ASCE/ASME Mechanics Conference, San Diego, California, July 9–12, 1989.

1.19 Arndt, N., Acosta, A.J., Brennen, C.E., and Caughey, T.K., "Wake Measurements for a Two–Dimensional Impeller," in preparation to be submitted for presentation at the Pumping Machinery Symposium at the Third Joint ASCE/ASME Mechanics Conference, San Diego, California, July 9–12, 1989.

Reports

2.1 Jery, B., and Franz, R., "Stiffness Matrices for the Rocketdyne Diffuser Volute," Report No. 249.1, Division of Engineering and Applied Science, California Institute of Technology, October 1982.

2.2 Chamieh, D.,"Forces on a Whirling Centrifugal Pump–Impeller," Ph.D. Thesis, Report No. 249.2, Division of Engineering and Applied Science, California Institute of Technology, 1983.

2.3 Adkins, D.R., "Analysis of Hydrodynamic Forces on Centrifugal Pump Impellers," Ph.D. Thesis and Report No. 200.23, Division of Engineering and Applied Science, California Institute of Technology, 1986.

2.4 Franz, R., and Arndt, N., "Measurements of Hydrodynamic Forces on the Impeller of the HPOTP of the SSME," Report No. 249.2, Division of Engineering and Applied Science, California Institute of Technology, 1986.

2.5 Arndt, N., and Franz, R., "Observations of Hydrodynamic Forces on Several Inducers Including the SSME LPOTP," Report No. 249.3, Division of Engineering and Applied Science, California Institute of Technology, 1986.

2.6 Franz, R., and Arndt, N., "Measurements of Hydrodynamic Forces on a Two–Dimensional Impeller and a Modified Centrifugal Pump," Report No. 249.4, Division of Engineering and Applied Science, California Institute of Technology, 1986.

2.7 Jery, B., "Experimental Study of Unsteady Hydrodynamic Force Matrices on Whirling Centrifugal Pump Impellers," Ph.D. Thesis and Report No. 200.22, Division of Engineering and Applied Science, California Institute of Technology, 1987.

2.8 Arndt, N., "Unsteady Impeller Blade–Diffuser Vane Pressure Measurements in a Diffuser Pump," Report No. 249.5, Division of Engineering and Applied Science, California Institute of Technology, January 1988.

12

2.9 Miskovish, R.S., and Brennen, C.E., "Some Unsteady Fluid Forces Measured on Pump Impellers," Report No. 249.6, Division of Engineering and Applied Science, California Institute of Technology, 1988.

2.10 Arndt, N., "Experimental Investigation of Rotor–Stator Interaction in Diffuser Pumps," Ph.D. Thesis and Report No. 249.7, Division of Engineering and Applied Science, California Institute of Technology, 1988.

2.11 Franz, R., "Experimental Investigation of the Effect of Cavitation on the Rotor-dynamic Forces on a Whirling Centrifugal Pump Impeller," (in preparation), Ph.D. Thesis and Report No. 249.8, Division of Engineering and Applied Science, California Institute of Technology, 1989.

APPENDIX B (PERSONNEL)

Principal Investigators

A.J. Acosta, Professor of Mechanical Engineering
C.E. Brennen, Professor of Mechanical Engineering
T.K. Caughey, Professor of Applied Mechanics

Graduate Students

D. Adkins, N. Arndt, D. Chamieh, R. Franz, B. Jery, F. Zhuang

Assistance was provided by

P.C. Chen, W. Goda, S. Ghosh, S. Moriarity, R.S. Miskovish, T. Tyler (undergraduate students, California Institute of Technology), M. Karyeaclis (graduate student, California Institute of Technology), D. Brennen (undergraduate student, University of California, San Diego)
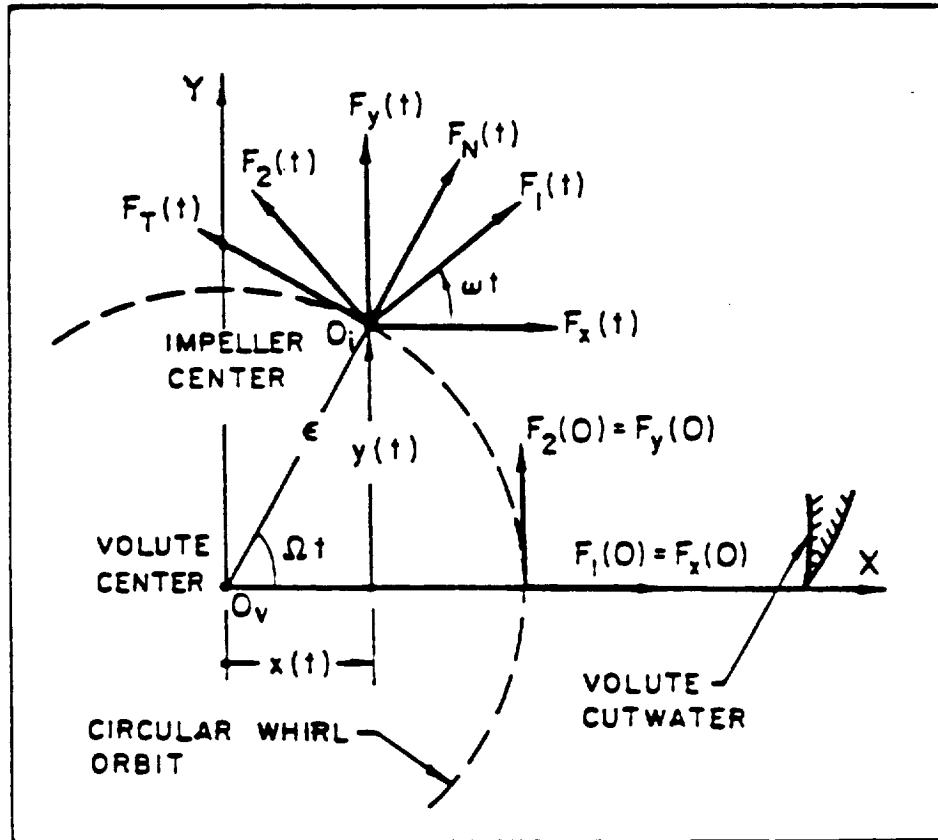
Figure 1. Schematic representation of the lateral forces in the rotating dynamometer frame (as F_1, F_2), in the stationary volute frame (as F_x, F_y) and in the local polar coordinate frame (as F_n, F_t).
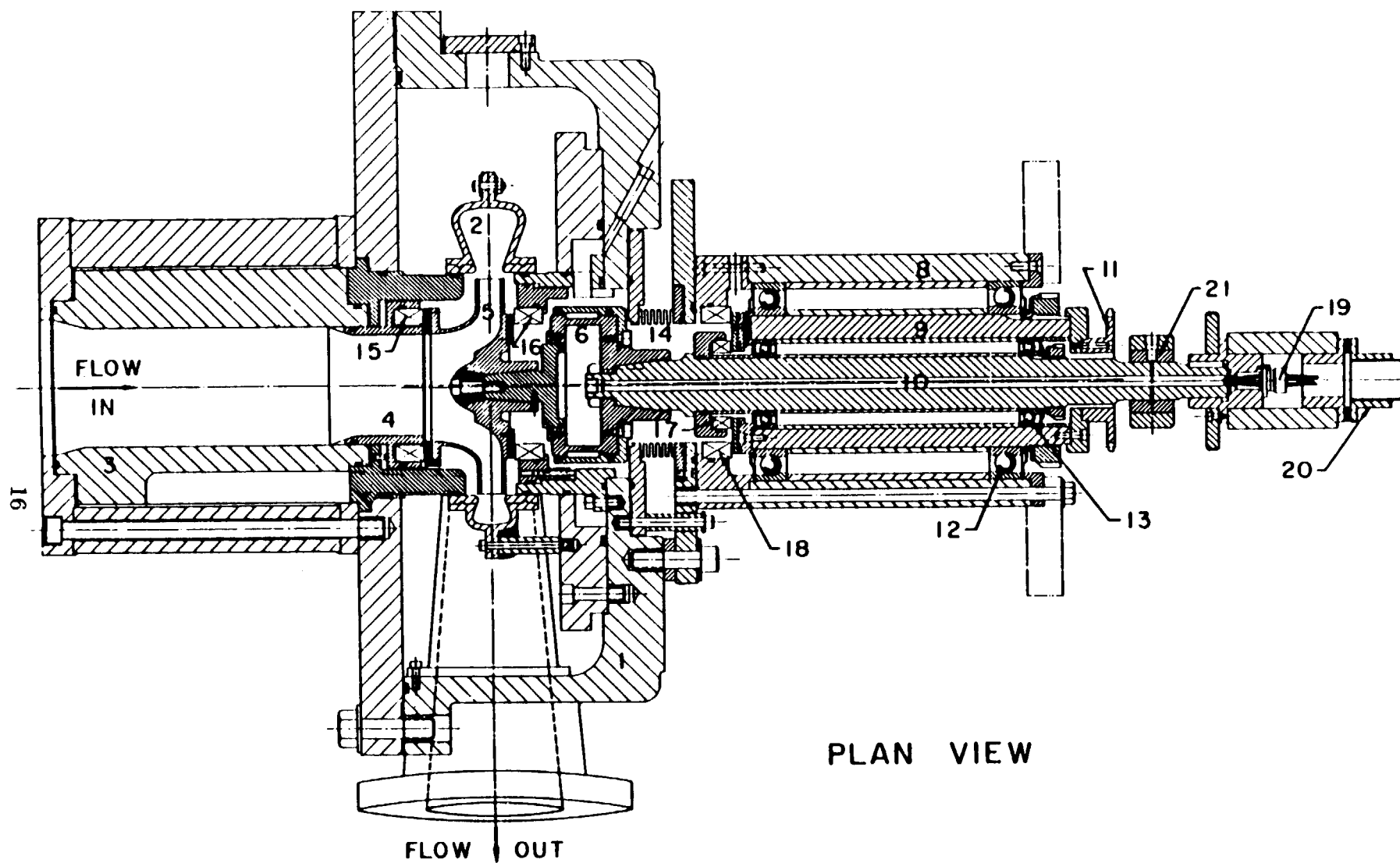
FLOW
IN

FLOW OUT

PLAN VIEW

Figure 2. Assembly drawing of the test section and the eccentric drive mechanism. Pump housing (1), volute (2), inlet connection (3), inlet bell (4), impeller (5), rotating dynamometer (6), eccentric drive mechanism: outer and inner bearing carriers (8 and 9), main shaft (10), orbiting motion sprocket (11), outer and inner bearing sets (12 and 13), bellows (14), impeller front and back (removed) face seal (15 and 16), eccentric drive inner and outer face seals (17 and 18), strain gage cable connecter (19), flexible coupling (20), and air bearing stator (21).